Dislocations under gradient flow and their effect on the renormalized coupling

Anna Hasenfratz[*] and Oliver Witzel[†]
Department of Physics, University of Colorado, Boulder, Colorado 80309, USA

(Received 10 April 2020; accepted 26 January 2021; published 12 February 2021)

Nonzero topological charge is prohibited in the chiral limit of continuum gauge-fermion systems because any unpaired instanton would create a zero mode of the Dirac operator. On the lattice, however, the geometric $Q_{\rm geom} = \langle F\tilde{F}\rangle/32\pi^2$ definition of the topological charge does not necessarily vanish in the chiral limit even when the gauge fields are smoothed for example with gradient flow. Small vacuum fluctuations (dislocations) not seen by the fermions may be promoted to instantonlike objects by the gradient flow. We demonstrate that these artifacts of the flow cause the gradient flow renormalized gauge coupling to increase and appear to run faster. In step-scaling studies such strong coupling artifacts contribute a term that might not follow perturbative scaling. The usual $a/L \to 0$ continuum limit extrapolations can hence lead to incorrect results. In this paper we investigate these topological lattice artifacts in the massless SU(3) 10-flavor system with domain wall fermions and the massless 8-flavor system with staggered fermions. For both systems we observe that in the range of strong coupling Symanzik gradient flow exhibits more lattice artifacts compared to Wilson gradient flow. We demonstrate how this artifact impacts the determination of the renormalized gauge coupling and the step-scaling β function.

DOI: 10.1103/PhysRevD.103.034505

I. INTRODUCTION

The nonperturbative determination of the renormalization group (RG) β function of gauge-fermion systems is essential to distinguish conformal and chirally broken systems, predict anomalous dimensions of infrared fixed points (IRFPs), determine the energy dependence of the running coupling, or predict α_s in quantum chromodynamics (QCD). Lattice calculations often aim to achieve these goals by calculating the step-scaling function, the lattice analogue of the RG β function of the gradient flow (GF) renormalized coupling $g^2_{\rm GF}$ [1–3]. While the GF coupling is fairly simple to obtain numerically, it can exhibit large lattice artifacts that complicates taking the continuum limit of the step-scaling function [4–14]. The situation is particularly difficult in systems near or inside the conformal window where the coupling runs very slowly. Simulations have to be pushed to strong bare coupling where vacuum fluctuations can be large, introducing cutoff effects that are not described by leading order perturbative predictions. In particular it may be difficult to distinguish cutoff effects from topological excitations. Especially on larger lattice sizes needed to take the continuum limit, this issue can become severe.

The geometric definition of the topological charge

$$Q_{\rm geom} = \frac{1}{32\pi^2}\int dx\, {\rm tr}(F_{\mu\nu}(x)\tilde{F}_{\mu\nu}(x)) \tag{1}$$

correctly separates the different topological sectors if the gauge field configurations are sufficiently smooth [15,16]. The "admissibility condition" however is not satisfied on configurations of typical lattice simulations. Cooling, smearing, and most recently gradient flow transformations have been used to suppress vacuum fluctuations and "reveal" the topological structure of configurations [17–25]. Unfortunately the predicted $Q_{\rm geom}$ value may depend on the details of the smoothing transformation. Small instantons may "fall through the lattice" for some smoothing transformation, while other transformations may promote certain vacuum fluctuations, "dislocations," to instantonlike objects [19]. In simulations with chirally symmetric fermions on lattices with (anti)periodic boundary conditions the index theorem offers an alternative definition of the topological charge [26,27]

$$Q_{\rm ferm} = \frac{1}{2}{\rm tr}(\gamma_5 D), \tag{2}$$

[*]anna.hasenfratz@colorado.edu
[†]Present address: Theoretische Physik 1, Naturwissenschaftlich-Technische Fakultät, Universität Siegen, 57068 Siegen, Germany. oliver.witzel@uni-siegen.de

Published by the American Physical Society under the terms of the Creative Commons Attribution 4.0 International license. Further distribution of this work must maintain attribution to the author(s) and the published article's title, journal citation, and DOI. Funded by SCOAP³.

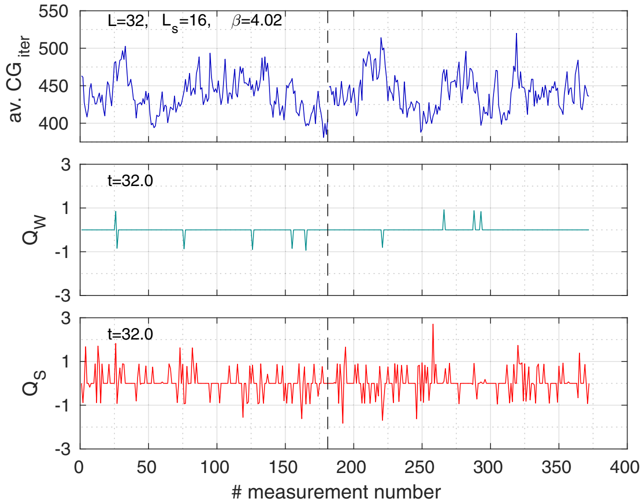

FIG. 1. Monte Carlo time histories of average number of CG iterations per molecular dynamics time step (top) and topological charge determinations after flow time $t/a^2 = 32$ using Wilson flow (middle) and Symanzik flow (bottom) for our strong coupling $(L/a)^4 = 32^4$ ensemble with $L_s = 16$ and $\beta = 4.02$. Measurements are performed every five trajectories. For further details see Sec. III A. The vertical dashed line separates data from two independent Monte Carlo streams.

the number of zero modes of the Dirac operator D. Q_{ferm} depends on the lattice Dirac operator but it does not require smoothing. The different definitions of the topological charge are expected to agree in the continuum limit but can be quite different on rough configurations [21,22,28–33].

There is a special situation where the topological charge can be predicted based on theoretical considerations. In systems where the index theorem is satisfied and the fermion mass vanishes, the zero modes of the Dirac operator are suppressed and $Q_{\mathrm{ferm}} = 0$ [26]. Any prediction of $Q_{\mathrm{geom}} \neq 0$ therefore signals a lattice artifact. On rough configurations e.g., in the strong coupling regime of near-conformal systems, this can occur frequently. To demonstrate the issue, we show in Fig. 1 Monte Carlo time histories for our massless ten flavor domain wall simulations [10,14] at the strong bare coupling $\beta = 4.02$ on $(L/a)^4 = 32^4$ lattices. Although the average number of conjugate gradient (CG) iterations per molecular dynamics time step fluctuates by less than $\pm 15\%$, we observe even after gradient flow time of $t/a^2 = 32$ nonzero predictions of the topological charge using Wilson flow (center) and Symanzik flow (bottom). The stability of the updating algorithm implies that the simulation does not encounter any zero modes of the fermion Dirac operator. Since on the same configuration, Wilson and Symanzik flow determine rather different values for the topological charge and combined with the observation that the number of CG iterations shows no substantial increase, we conclude that any nonzero value of the topological charge reported by either Wilson of Symanzik flow is a lattice artifact.

We investigate the consequences of such lattice artifacts on the GF renormalized coupling and the step-scaling function. We find that the gradient flow coupling g^2_{GF} receives a positive contributions from topological objects. This translates to a positive contribution to the discrete lattice β function, consistent with the findings of Ref. [34]. We observe that different flow kernels may identify different topological charge on the same configurations. Among the commonly used gradient flow choices, Wilson flow tends to have the least topological artifacts, Symanzik flow more and Iwasaki flow much more, similarly to observations in cooling [19]. This is not surprising as gradient flow and cooling are closely connected [25].

In this paper we reanalyze data from simulations performed at strong coupling where the gauge fields are rough and dislocations frequent. Such simulations are necessary to explore the step-scaling function of (near) conformal systems. This phenomena might also affect scale setting [3,35,36] in strongly coupled beyond the Standard Model systems (see e.g., [37–50]) or even QCD simulations at coarse lattice spacings necessary to achieve a large physical box needed e.g., to study multiparticle interactions [51].

We consider two different systems to illustrate the issue. In both cases we study two different gradient flow kernels, Wilson and Symanzik flow. We start with our recent 10-flavor SU(3) domain wall simulations where we first observed the effect of nonzero topological charge [10]. An accompanying paper discusses the step-scaling function of this most likely conformal system and provides further details [14]. Next we analyze configurations generated for an older study of the SU(3) 8-flavor system with staggered fermions [6]. We chose these two systems because both simulations have been pushed toward very strong coupling where the contamination from topological modes can be significant. Our results demonstrate these lattice artifacts are more severe for Symanzik than for Wilson flow. In Sec. V we demonstrate how a small modification of the flow kernel results in a gradient flow that is better at smoothing out local dislocations resulting in fewer configurations with nonzero topological charge. The lattice discretization errors of such a modified gradient flow will need to be explored in the future. We also consider filtering to the $Q_{\mathrm{geom}} = 0$ sector as proposed in Ref. [34] and successfully applied by the Alpha collaboration [7]. Finally we briefly summarize our findings.

II. TOPOLOGY AND THE STEP-SCALING FUNCTION

The GF gauge coupling at energy scale $\mu = 1/\sqrt{8t}$ is defined as $g^2_{\mathrm{GF}}(t; L, \beta) = \mathcal{N} t^2 \langle E \rangle$ where $\langle E \rangle$ is the energy density and t the GF time. $\beta = 6/g_0^2$ is the bare coupling, L refers to the linear size of the system, and the normalization factor $\mathcal{N}$ is chosen to match $g^2_{\overline{\mathrm{MS}}}$ at one-loop [1–3]. Lattice studies show that at large flow time $g^2_{\mathrm{GF}}(t)$ exhibits only mild, approximately linear or weaker, dependence on t, suggesting that the energy density $\langle E\rangle$ decreases $\propto 1/t$ or faster. While GF removes vacuum fluctuations and instanton pairs, some dislocations/instantons can survive the flow and become (quasi-)stable. At large flow time Q_{geom} approaches integer values and $\langle Q^2_{\mathrm{geom}}\rangle$ is frequently used to define the lattice topological susceptibility $\chi_T = \langle Q^2_{\mathrm{geom}}\rangle/V$ where V is the volume of the system [23,24,32,33].

In the continuum the action of a single instanton is $S_I = 8\pi^2$. Due to discretization effects on the lattice this value depends on the instanton size and the lattice action, but at large flow time smooth instantons increase the energy of the configuration by $\approx S_I$ [22]. The absolute value of the topological charge $\langle |Q|\rangle$ is expected to scale with the square root of the volume times χ_T.[1] Therefore the instanton contribution to the energy density is

$$\langle E_Q\rangle \propto \frac{S_I\langle|Q|\rangle}{V} \propto \sqrt{\chi_T V}/V = \sqrt{\chi_T/V}. \tag{3}$$

If instanton–anti-instanton pairs are present, this value is even larger.

In step-scaling studies the GF flow time is tied to the system size as $t = (cL)^2/8$, where the constant c defines the renormalization scheme. The finite volume discrete β function of scale change s is defined as [4]

$$\beta_{c,s}(g_c^2; L, \beta) = \frac{g_c^2(sL;\beta) - g_c^2(L;\beta)}{\log s^2}, \tag{4}$$

where g_c^2 refers to the gradient flow renormalized coupling at the corresponding flow time $g^2_{\mathrm{GF}}(t; L, \beta)$. In volumes $V = L^4$ the contribution of the instantons to the discrete β function therefore is $\mathcal{N} t^2\langle E_Q\rangle \propto \langle|Q|\rangle \propto \sqrt{\chi_T} L^2$. We may separate the $Q = 0$ and $Q \neq 0$ contributions to the β function and write

$$\beta_{c,s}(g_c^2; L, \beta) = \beta_{c,s}(g_c^2)_{Q=0} + \mathcal{C}L^2, \tag{5}$$

where $\beta_{c,s}(g_c^2)_{Q=0}$ is the step-scaling function in the $Q = 0$ sector and the mass square dimension quantity $\mathcal{C} \propto \sqrt{\chi_T}$ is independent of the system size L. In the continuum limit, $\mathcal{C}L^2$ takes a finite value and simply shifts the finite volume step-scaling function $\beta_{c,s}$.

When the simulations are performed with chirally symmetric fermions in the $m = 0$ chiral limit and on periodic volumes, any nonvanishing value for $\mathcal{C}L^2$ signals a lattice artifact, the consequence of the GF promoting vacuum fluctuations (dislocations) to topological objects. In this case instead of $\mathcal{C}L^2 \propto \langle|Q|\rangle$, the correction to the finite volume β function depends on the square root of the number of dislocations that does not scale with any known power of the lattice spacing. While this lattice artifact vanishes in the continuum limit as the bare coupling is tuned to the perturbative fixed point, it can alter the lattice predictions at strong coupling. For example, at the infrared fixed point of a conformal system $\beta_{c,s}(g_c^2)_{Q=0} = 0$ but $\mathcal{C}L^2 > 0$ suggests an incorrect positive β function. In the vicinity of the IRFP small changes of the bare coupling can lead to a large change in the lattice spacing a. At the same time vacuum fluctuations creating dislocations might not change much, and the number of dislocations increase with the square root of the number of lattice sites, i.e., $\mathcal{C}L^2 \propto \sqrt{(L/a)^4}$ could increase as $1/a^2$.

Even on $Q = 0$ configurations, $\beta_{c,s}(g_c^2)_{Q=0}$ has cutoff effects. These are typically removed by an $a^2/L^2 \to 0$ extrapolation at fixed renormalized coupling g_c^2 [4–10,13]. If the data does not follow a^2/L^2 dependence, higher order $(a/L)^4$ terms can be included [11,12]. However, in the vicinity of an IRFP and if $\mathcal{C}L^2$ increases as a decreases, a continuum extrapolation of $\beta_{c,s}(g_c^2; L, \beta)$ in $a^2/L^2 \to 0$ is not viable. This reflects the nonperturbative nature of dislocations and shows that this effect cannot be removed by perturbatively motivated extrapolations. This lattice artifact can be a substantial contribution to $\beta_{c,s}(g_c^2; L, \beta)$ resulting in a misleading continuum extrapolation. A clean way to avoid the issue is to choose a flow kernel where topological objects are not generated even on coarse lattices.

To simplify the notation we will from now on refer to Q_{geom} simply by using Q.

III. SU(3) WITH $N_f = 10$ FLAVORS

A. Details of the simulations

For this part of our study we utilize existing gauge field configurations generated with ten degenerate and massless flavors of three times stout-smeared [52] Möbius domain wall (DW) fermions [53–55] ($b_5 = 1.5$, $c_5 = 0.5$) with Symanzik gauge action [56,57]. The configurations are generated using GRID [58,59] and we choose symmetric volumes with $V = L^4$ where the gauge fields have periodic, the fermions antiperiodic boundary conditions in all four space-time directions. The bare input quark mass is zero and for the domain wall fermions we choose the domain wall height $M_5 = 1$ and the extent of the fifth dimension $L_s = 16$. Configurations are generated using the hybrid Monte Carlo update algorithm [60] choosing trajectories of length two molecular time units (MDTU) and we use configurations saved every 10 MDTU. Our statistical data analysis is performed using the Γ-method [61] which estimates and accounts for integrated autocorrelation times. For the $L/a = 32$ ensembles at strong coupling considered here autocorrelations range from three to five measurements.

[1] If the distribution of the topological charge is Gaussian $n_Q \propto e^{-Q^2/c}$, $\langle|Q|\rangle = \sqrt{2\langle Q^2\rangle/\pi}$.

Due to the finite extent of the fifth dimension, DW fermions exhibit a small, residual chiral symmetry breaking which conventionally is parametrized by an additive mass term $am_{\rm res}$. We determine am_{res} numerically using the ratio of midpoint-pseudoscalar and pseudoscalar-pseudoscalar correlator. At strong coupling $am_{\rm res}$ depends on the bare coupling β and increases from $am_{\rm res} = 2\times10^{-5}$ at $\beta = 4.15$ to 6×10^{-4} at $\beta = 4.02$. To demonstrate that $am_{\rm res}$ is sufficiently small and not the origin of nonzero topological charges, we compare results for $\beta = 4.05$ from ensembles with $L_s = 16$ and $L_s = 32$ below.

B. Effects of nonzero topological charge

We illustrate the effects of $Q \neq 0$ instantonlike objects on the gradient flow coupling in Fig. 2 where we show the flow time dependence of the topological charge Q and the GF coupling $g^2_{\rm GF}$ on six individual configurations. We use the clover operator to approximate $F\tilde{F}$ in Eq. (1). The upper panels in each subfigure show the flow time evolution of the topological charge both with Wilson (W) and Symanzik (S) flows. The lower panels show the renormalized $g^2_{\rm GF}$ coupling evaluated with both the Wilson plaquette (W) and clover (C) operators for both flows.[2] The six configurations were chosen to illustrate the difference between $Q = 0$ and $Q \neq 0$. They are part of our $N_f = 10$ DW ensemble at $\beta = 4.02$, the strongest bare coupling we consider, on 32^4 volumes [14]. The topological charge shows large fluctuations at small flow time but settles to a near-integer value by $t/a^2 \gtrsim 5.0$. We observe occasional changes in Q for $t/a^2 > 5$ but these tend to be quick as topological objects are annihilated by the flow.

At large flow time we expect different flows and operators to converge. That is indeed the case at trajectory #700 and #575 (top left and top right in Fig. 2) where, as shown in the upper panels, Wilson and Symanzik flows find the same topological charge at large flow time. Both Wilson and Symanzik flows as well as Wilson and clover operators predict consistent $g^2_{\rm GF}$ at large flow time, as is shown on the lower panels.

At trajectory #2965 and #2100 (middle of Fig. 2) Wilson flow predicts $Q = 0$ but Symanzik flow identifies topological charge $Q = 2$ and -2, respectively. With Wilson flow, $g^2_{\rm GF}$ shows a flat, slowly decreasing behavior with flow time, similar to what is observed at trajectory # 700 with $Q = 0$. Symanzik flow, however, shows $g^2_{\rm GF}$ increasing roughly linearly with the flow time, similar to trajectory # 575, $Q = -1$, although the slope is larger, consistent with two topological objects on the configurations. Different operators are still consistent within each flow.

At trajectory #2255 (bottom left) and #845 (bottom right) the topological charge with Wilson flow is $Q = 0$ but with Symanzik flow we see a rapid change at larger flow time. At trajectory #2255 this corresponds to $Q = -1 \to Q = 0$ around $t \approx 26$. Correspondingly $g^2_{\rm GF}$ changes from a linearly increasing flow time dependence to a flat/decreasing form. At trajectory #845 the change is $Q = 0 \to Q = -1$, suggesting that the configuration at flow time $t/a^2 < 12$ had an instanton–anti-instanton pair. The instanton is annihilated by the flow at $t/a^2 \approx 13$, leaving the anti-instanton unpaired. The renormalized coupling $g^2_{\rm GF}$ follows the expected behavior. Its linear rise with the flow time slows at $t/a^2 \approx 13$ but remains linear, similar to what is observed at trajectory #575.

Any non-vanishing Q is an artifact of the gradient flow in simulations with massless chirally symmetric fermions. The panels of Fig. 2 verify that on $Q \neq 0$ configurations $g^2_{\rm GF}$ receives a contribution that increases approximately linearly with flow time and $|Q|$. Next we investigate what fraction of the configuration ensembles is affected by this lattice artifact. In Fig. 3 we show the flow time evolution of the topological charge defined by Eq. (1) on a subset of our $N_f = 10$, 32^4 configurations at bare coupling $\beta = 4.02$, 4.05, 4.10 and 4.15. Each panel includes 100 configurations, separated by 10 MDTU, analyzing Wilson flow data on the left, Symanzik flow data on the right. The vertical lines indicate flow times $t/a^2 = 8.0$ and 11.52 which correspond to $c = 0.25$ and 0.3 in step-scaling studies.

At small flow time, vacuum fluctuations dominate Q. At the weaker couplings, $\beta = 4.15$, 4.10, most vacuum fluctuations die out by $t/a^2 \gtrsim 2$, and while Q may not exactly be integer, it is close to an integer $(0, \pm1, \pm2, \ldots)$. It is well known that different gauge actions suppress/promote dislocations differently [21,22]. The gradient flow has a similar dependence of the flow action. With Wilson flow most configurations have $Q = 0$. Symanzik flow sustains $Q \neq 0$ longer, and one of the 100 $\beta = 4.10$ configurations remains at $Q = -1$ even at $t/a^2 = 32$, our maximal flow time. The picture changes rapidly toward strong coupling. At our strongest gauge coupling $\beta = 4.02$ even Wilson flow has several $Q \neq 0$ configurations at $t/a^2 \approx 10$, some surviving even at $t/a^2 = 32$. Symanzik flow enhances this lattice artifact even further. The topological charge distribution of Symanzik flowed configurations resemble QCD at finite mass however here $Q \neq 0$ signals only lattice artifacts.

At large flow time it is possible to filter configurations according to different topological sectors [7]. Analyzing only those with $Q = 0$ and contrasting the predictions with the full data set provides information on the effect of $Q \neq 0$. In Fig. 4 we compare the finite volume step-scaling $\beta_{c,s}(g^2_c)$ functions defined in Eq. (5) with and without topological filtering. The plots show $\beta_{c,s}$ predicted by the lattice volumes $L/a = 16 \to 32$ on the $\beta = 4.02$ configuration set as the function of $c = \sqrt{8t}/L$ with Wilson flow (left) and Symanzik flow (right), using the Wilson plaquette operator to predict the energy density. While in the Wilson

[2]The first letter shorthand notation indicates the gradient flow (W or S), the second letter the operator (W or C).

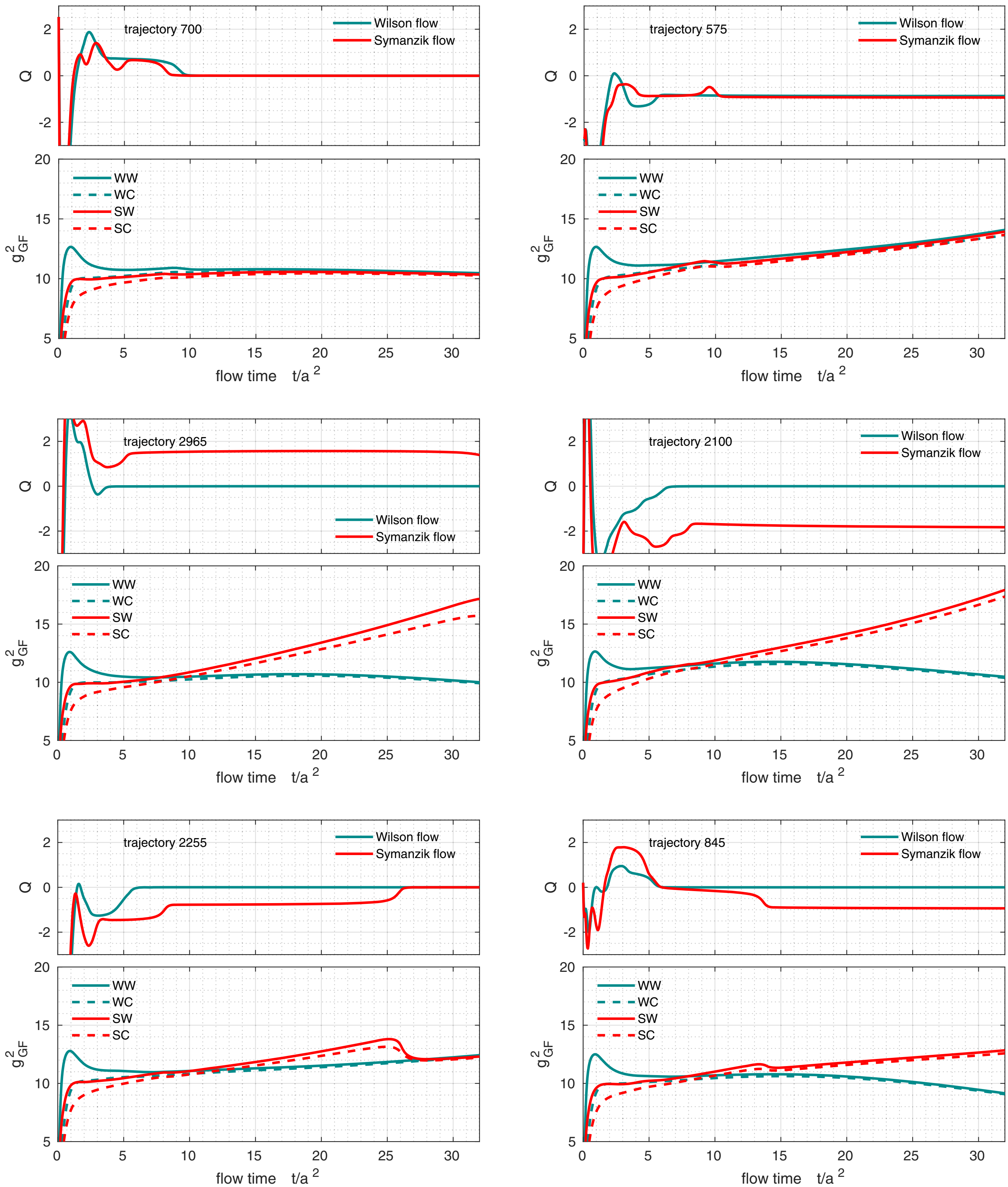

FIG. 2. The flow time history of the topological charge (upper panels) and the gradient flow coupling (lower panels) on six selected gauge field configurations of our ten flavor $(L/a)^4$ ensembles with $L/a = 32$, $L_s = 16$ at bare coupling $\beta \equiv 6/g_0^2 = 4.02$. We show both Wilson (green) and Symanzik (red) flow and determine the gradient flow coupling for the Wilson-plaquette (W, solid lines) and clover (C, dashed lines) operator.

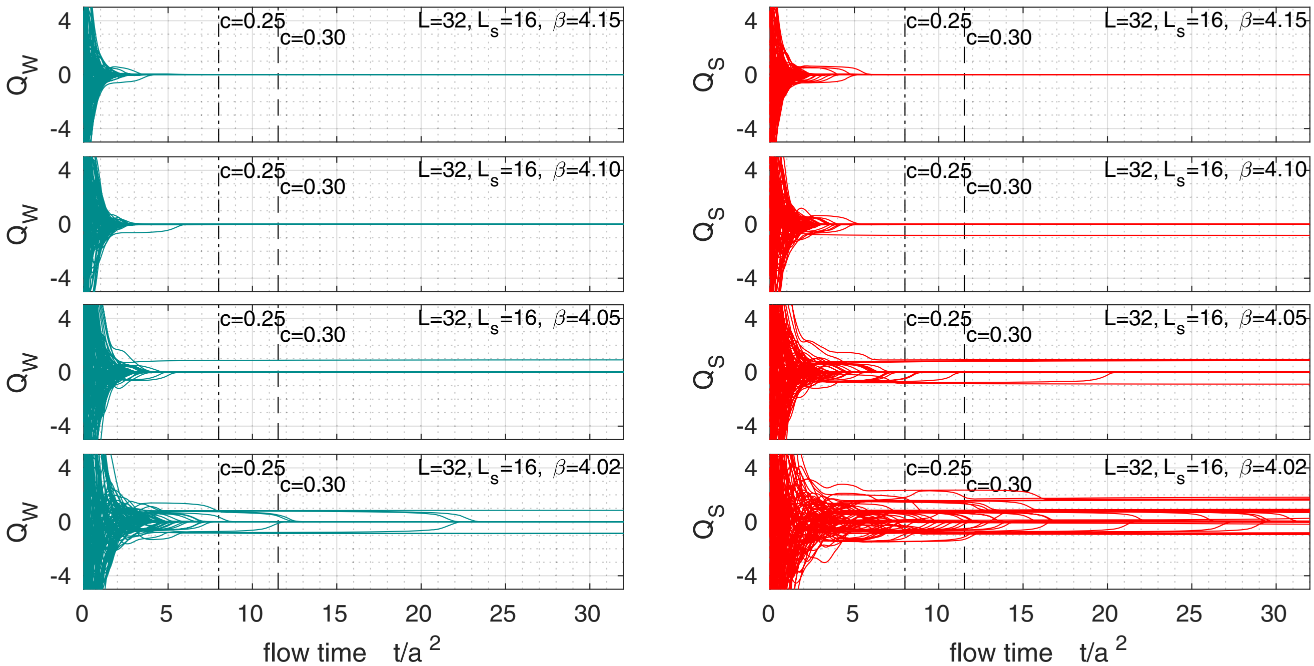

FIG. 3. Dependence of the topological charge Q on the flow time t/a^2 for $(L/a)^4 = 32^4$ ensemble with $L_s = 16$ and at bare couplings $\beta = 4.15$, 4.10, 4.05, and 4.02. Each panel shows the flow time histories for the first thermalized 100 configurations of each ensemble. The left (right) panels show the flow time histories using Wilson (Symanzik) gradient flow. Lattice artifacts in the form of nonzero topological charges Q increase in the strong coupling limit (decreasing β) and are more pronounced for Symanzik than for Wilson flow.

flow analysis filtering on the topology has only a minimal effect, the $Q = 0$ subset with Symanzik flow predicts a significantly slower running step-scaling function.[3] This is consistent with the observation we made in connection with Fig. 2 where we pointed out that $Q \neq 0$ configurations have faster running gauge coupling $g^2_{\rm GF}$. This effect weakens at weak gauge coupling and does not change the continuum limit if the ensembles used in the a^2/L^2 extrapolation are at sufficiently weak coupling. In the strong coupling regime where the data are contaminated by dislocation artifacts, we expect that the a^2/L^2 or a^4/L^4 extrapolated step-scaling functions overestimates the running of the gauge coupling, especially with Symanzik flow. In the accompanying paper [14] we show details of our analysis.

We close our discussion with Fig. 5 where we compare g^2_c for $c = 0.300$ as predicted by configurations with $|Q| = 0$, 1 and 2 on our $\beta = 4.02$ data set. As expected based on Eq. (5) and Figs. 2 and 4, g^2_c increases with $|Q|$. On the right side panel of Fig. 5 we show the relative weight of the different topological sectors. In the case of Symanzik flow we analyze 371 measurements in total, 211 with $|Q| = 0$, 143 with $|Q| = 1$ and 17 with $|Q| = 2$ but do not show one measurement with $|Q| > 2$. In the case of Wilson flow we analyze 353 configurations with $|Q| = 0$ and 19 with $|Q| = 1$. Differences between WW and SW determinations of g^2_c indicate cutoff effects which are only supposed to disappear after taking the continuum limit.

Measuring the total topological charge Q does not give information on possible instanton–anti-instanton pairs. However the change of the slopes of $g^2_{\rm GF}$ observed in Fig. 2 suggests that most $Q \neq 0$ configurations have only isolated instantons and not many pairs. Our analysis filtering on the topological charge is similar to the suggestion of Ref. [7] and could be considered as an alternative method to predict the running coupling and the step-scaling function.

C. Finite value of L_s

Stout smeared Möbius domain wall fermions with $L_s = 16$ have a small residual mass, $am_{\rm res} < 10^{-3}$ even at our strongest gauge coupling. We check for possible effects due to nonvanishing residual mass by generating a second ensemble at bare coupling $\beta = 4.05$ with $L_s = 32$. The numerical cost of generating an $L_s = 32$ trajectory is more than five times greater compared to the simulation with $L_s = 16$. Thus we have fewer $L_s = 32$ trajectories (about $1/3$) than for $L_s = 16$. In Fig. 6 we show the flow time histories for the topological charge Q for the first 100 configurations of each ensemble. While Wilson flow identifies very few configurations with nonzero Q on either

[3]We define the integer topological charge as the integer part of $(|Q_{\rm geom}| + 0.5)$ where $Q_{\rm geom}$ is the value predicted by the clover $F\tilde{F}$ operator. At large flow time $Q_{\rm geom}$ is close to an integer, apart from the regions where the topological charge undergoes a rapid change.

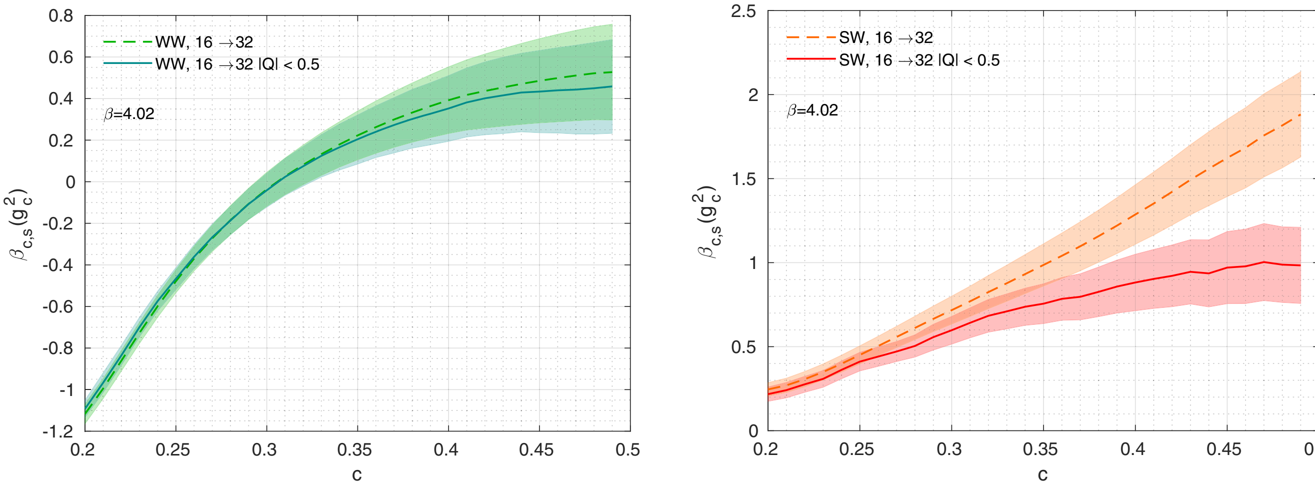

FIG. 4. Effect of nonzero topological charge Q on the value of the step-scaling $\beta_{c,s}$ function determined from the Wilson plaquette operator for the $16 \to 32$ volume pair ($s = 2$) at bare coupling $\beta \equiv 6/g_0^2 = 4.02$ as function of the renormalization scheme parameter c, which is related to the flow time t. Since at $\beta = 4.02$ Wilson flow exhibits in total only three configurations where a nonzero topological charge is measured, filtering configurations with $|Q| < 0.5$ does not impact the prediction of $\beta_{c,s}$ (left panel). For Symanzik flow (right panel), however, a large number of configurations with nonzero topological charge are found, resulting in a larger $\beta_{c,s}$ compared to the analysis using only $|Q| < 0.5$. The discrepancy grows with c.

ensembles, the same ensembles exhibit more nonzero topology under Symanzik flow. Surprisingly, the relative number of configurations with nonzero Q more than triples under Symanzik flow when L_s increases from 16 to 32. This observation again indicates that nonvanishing

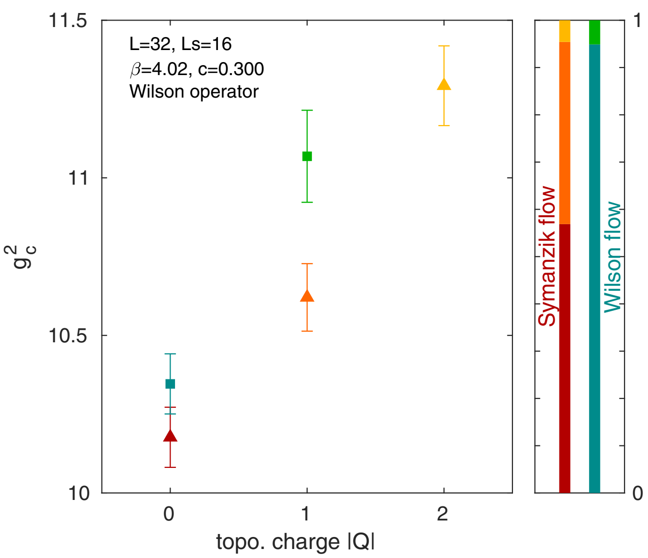

FIG. 5. On the left: renormalized coupling g_c^2 as predicted by Symanzik (red/orange/yellow triangles) and Wilson (green squares) flows and Wilson operator on configurations with $|Q| = 0$, 1, and 2 at $c = 0.300$ (GF flow time $t = 11.52$). The panel on the right shows the relative fraction of configurations at each $|Q|$ sector when using Symanzik and Wilson, respectively. In total 371 (372) configurations enter the presented results for Symanzik (Wilson) flow.

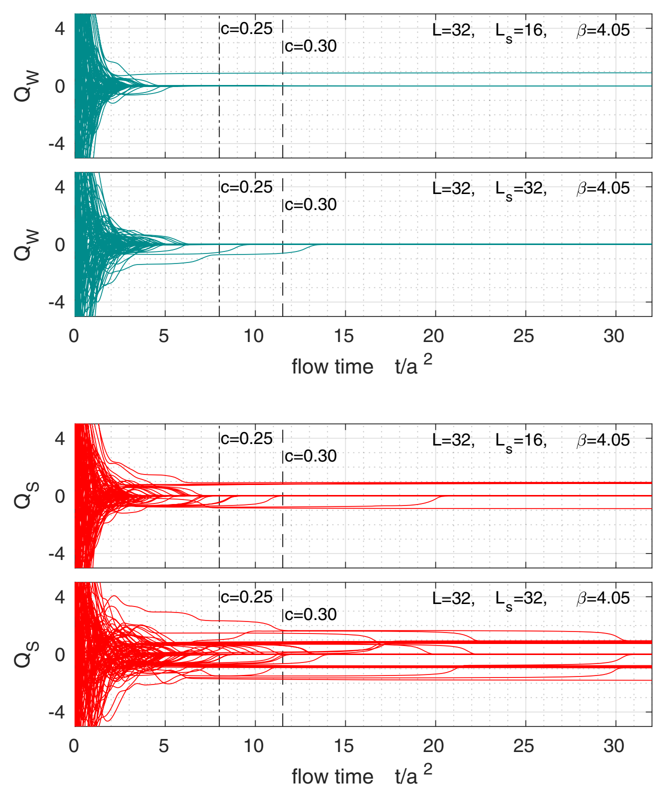

FIG. 6. Comparison of flow time histories of the topological charge Q for the first 100 thermalized configurations of the $\beta = 4.05$ ensembles with $L_s = 16$ and $L_s = 32$. The upper two panels show Q_W determined with Wilson flow (W), the lower two panels show Q_S determined with Symanzik flow (S). In each case, the $L_s = 16$ data are shown above the $L_s = 32$ data.

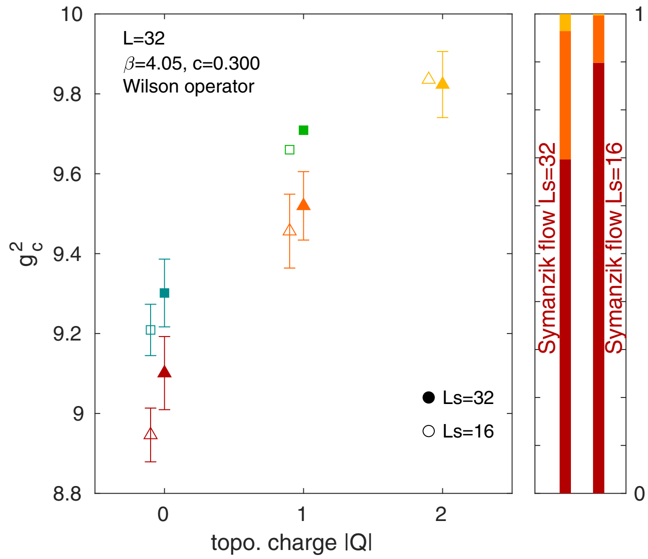

FIG. 7. Renormalized coupling g_c^2 for the renormalization scheme $c = 0.30$ determined on $L/a = 32$ ensembles at $\beta = 4.05$ for ensembles with $L_s = 16$ (open symbols) and $L_s = 32$ (filled symbols). In case of Wilson flow (green squares) only a value for configurations with $|Q| = 0$ can be determined, whereas for Symanzik flow (red/orange/yellow triangles) g_c^2 for $|Q| = 0$, 1 sectors can be determined at $L_s = 16$ and in addition $|Q| = 2$ for $L_s = 32$. All g_c^2 values at the same $|Q|$ agree perfectly which strongly implies effects due to $L_s = 16$ are not resolved within our statistical errors. For Symanzik flow, however, each $|Q|$ sector predicts a statistically different value of g_c^2. The relative distribution of the $|Q|$ sectors for Symanzik flow are shown in the small panel on the right. For $L_s = 16$ in total 372 measurements are analyzed, for $L_s = 32$ 112.

topology is an artifact of the flow and not due to the small residual mass.

Next we determine the renormalized coupling g_c^2 for the renormalization scheme $c = 0.300$ on both ensembles where we again separate configurations according to the value of $|Q|$. The outcome is shown in Fig. 7. On both ensembles Wilson flow (green squares) predominantly finds zero topological charge and identifies too few configurations with $|Q| = 1$ to reliably estimate an uncertainty on g_c^2. Hence we show the values for $|Q| = 0$ with statistical error bar but indicate only the central values at $|Q| = 1$. The prediction on the $L_s = 16$ ensemble (open symbol) is in perfect agreement with the $L_s = 32$ ensemble (filled symbol). For Symanzik flow (red/orange/yellow triangles) we find several configurations with $|Q| = 0$ and 1 plus one configuration with $|Q| = 2$ on the $L_s = 16$ ensemble and several configurations in all three sectors for $L_s = 32$. The g_c^2 values clearly resolve a dependence on Q. At the same time, we observe good agreement for g_c^2 predicted at the same value of Q on ensembles with different L_s. The latter strongly implies that the effect of choosing $L_s = 16$ vs $L_s = 32$ is negligible within our statistical uncertainties. The relative distribution of the $|Q|$ sectors for Symanzik flow are shown in the small panel on the right of Fig. 7. For $L_s = 16$ in total 372 measurements are analyzed and 90% have $Q = 0$. For $L_s = 32$ we analyze 112 measurements but only 70% have $|Q| = 0$. Since $|Q| > 0$ predict larger g_c^2, the average of the renormalized coupling increases with increasing L_s. However, this is an artifact of the flow and implies larger lattice artifacts for larger L_s.

IV. SU(3) WITH $N_f = 8$ FLAVORS

A. Details of the simulations

In this part of our study we utilize existing gauge field configurations generated with eight degenerate and massless flavors of staggered fermions with nHYP smeared links [62,63] and gauge action that combines plaquette and adjoint plaquette terms [6]. The configurations have symmetric volumes, $V = L^4$, where the gauge fields have periodic boundary conditions and the fermions antiperiodic boundary conditions in all four space-time directions. Apart from the boundary conditions this is the same action used in the large scale studies of Refs. [43,64].

Staggered fermions have a remnant U(1) chiral symmetry that protects the fermion mass from additive mass renormalization. On the other hand taste breaking of staggered fermions split the eigenmodes of the Dirac operator. Smooth, isolated instantons have four near-zero eigenmodes for the four staggered species, but they are split into two positive, two negative imaginary eigenvalue pairs. The determinant of the Dirac operator is not exactly zero, topologically nontrivial configurations are not prohibited. In the continuum limit taste symmetry is recovered and $Q \neq 0$ configurations should be suppressed. Therefore it is reasonable to consider all $Q \neq 0$ as lattice artifact—either from the action or from the flow.

B. Effects of nonzero topological charge

Our discussion and analysis here follows that of Sec. III with domain wall fermions. The strongest gauge coupling of the simulations with one level of nHYP smearing is $\beta = 5.0$, and the largest volume has $L/a = 30$. In Fig. 8 we show the evolution of the topological charge with Wilson and Symanzik flow on 50 thermalized consecutive configurations at $\beta = 5.0$, 5.4 and 5.8. Similar to the DW result, we observe the emergence of more $Q \neq 0$ configurations at strong coupling. We also observe rapid changes in Q at large flow time, and again more $|Q| > 0$ with Symanzik than with Wilson flow. In Fig. 9 we compare the renormalized GF coupling in the $c = 0.300$ renormalization scheme for the different topological sectors. As in Fig. 5, we see a clear increase in g_c^2 as $|Q|$ increases. Since the fraction of $Q \neq 0$ configurations is much larger with Symanzik than Wilson flow, this implies that step-scaling studies using Symanzik flow may overestimate $\beta_{c,s}(g^2)$ at strong gauge coupling.

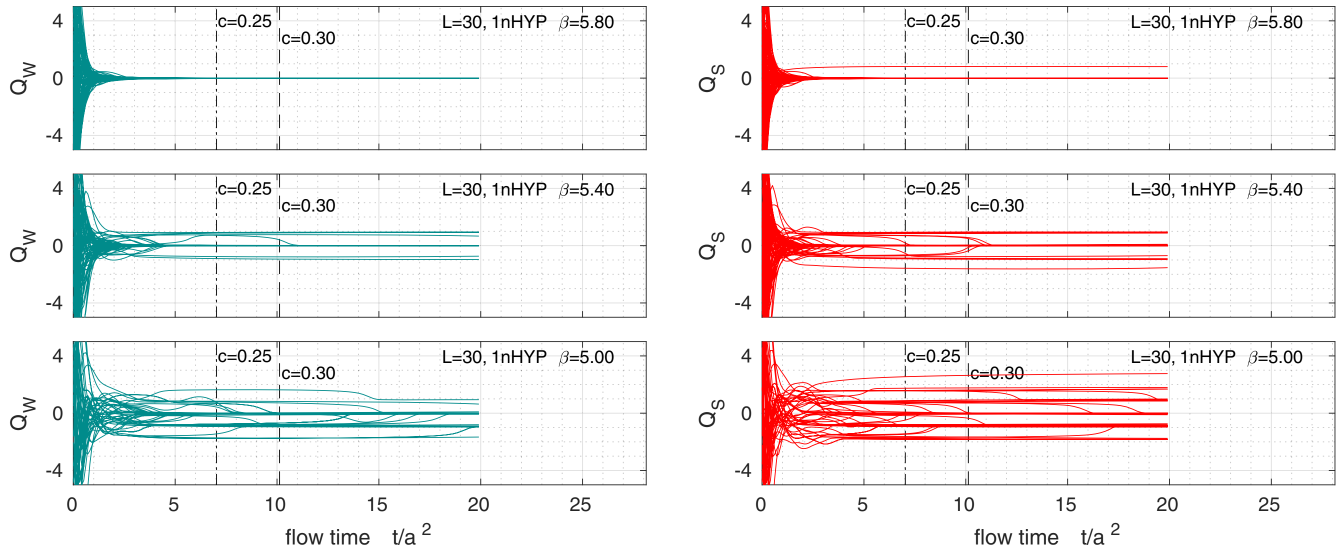

FIG. 8. Flow time histories for the $N_f = 8$ data set with one level of nHYP smeared staggered fermions on $(L/a)^4 = 30^4$ lattices at bare gauge coupling $\beta = 5.80, 5.40, 5.00$. Similar to $N_f = 10$ DW fermions (Fig. 2) we observe an increase of nonzero topology as β decreases and the suppression of topology is inferior for Symanzik compared to Wilson flow.

We note however the investigation in Ref. [6] studied this system using only Wilson flow. It would be very interesting to reanalyze the existing configurations not only with Symanzik flow, but also with a flow that suppresses the topology even further than Wilson flow.

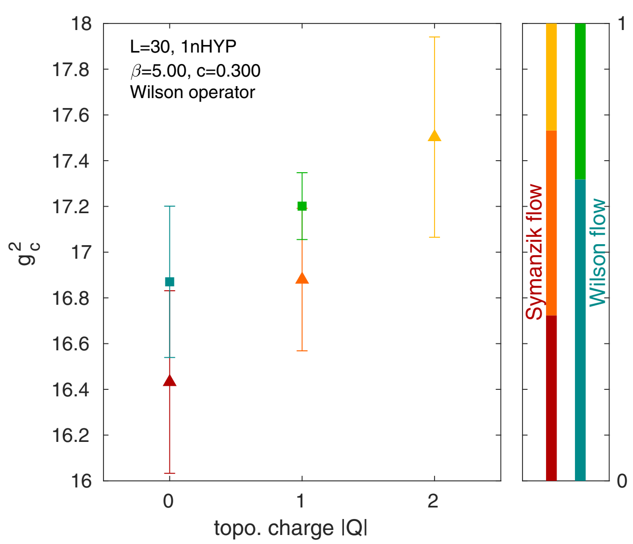

FIG. 9. Renormalized coupling g_c^2 determined for different topological sectors using the strongest coupling of the $N_f = 8$ staggered fermion ensemble at $\beta = 5.00$ and $c = 0.300$. g_c^2 increases with the charge Q, similar to DW in Fig. 5. Green squares correspond to Wilson flow, red/orange/yellow triangles to Symanzik flow. The relative fraction of each Q sector is shown by the panel on the right. Similar to the DW results, Symanzik flow creates more $Q \neq 0$ configurations than Wilson flow.

V. GRADIENT FLOW WITH IMPROVED TOPOLOGY SUPPRESSION

The flow kernel of Symanzik flow is a combination of a 1×1 plaquette and a 2×1 rectangle term, with coefficients $c_{1\times1} = 5/3$ and $c_{2\times1} = -1/12$. Wilson flow is performed only with the plaquette term i.e., $c_{1\times1} = 1$, $c_{2\times1} = 0$. Apparently the negative $c_{2\times1}$ term increases the probability of $Q \neq 0$ in Symanzik flow. This suggests that a positive

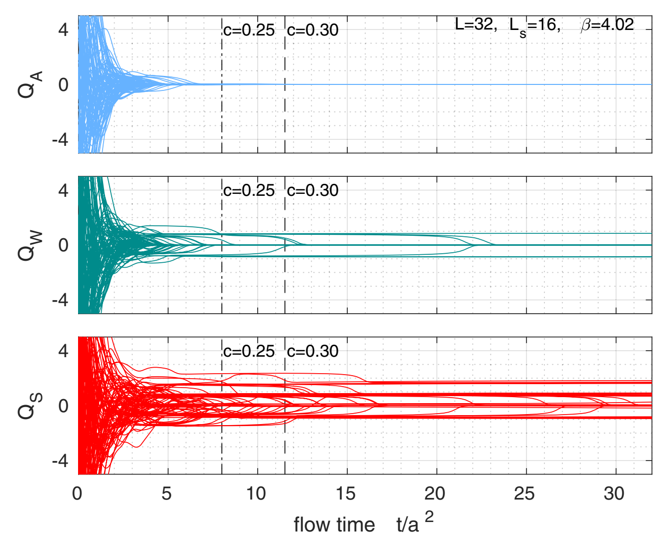

FIG. 10. Demonstration of the topology suppressing features of our alternative flow with positive coefficient for the 2×1 rectangle term. We explore this alternative GF using our $N_f = 10$ domain wall lattice with $L/a = 32$ at $\beta = 4.02$ and analyze again the first 100 thermalized configurations. The alternative flow (A) is shown on the top in blue and for easy comparison we repeat below Wilson flow (W, green) and Symanzik flow (S, red).

$c_{2\times 1}$ term might lead to a better suppression of this lattice artifact. To test the idea we implemented an alternative gradient flow (A) where we set the coefficients to

$$c_{1\times 1} = 2/3 \quad \text{and} \quad c_{2\times 1} = 1/24 \tag{6}$$

and demonstrate its effect on the topological charge Q using our $N_f = 10$ domain wall ensemble at bare coupling $\beta = 4.02$. In Fig. 10 we show how the suppression of the topological charge is improved with respect to Wilson and Symanzik flow. Whether or not this alternative gradient flow is a viable candidate to perform step-scaling studies at strong coupling will however require further investigations using multiple volumes and a range of bare coupling β. Only that will allow to estimate discretization effects to be removed by the continuum limit extrapolation.

VI. SUMMARY

In this paper we demonstrate that gradient flow measurements on rough gauge field configurations can promote lattice dislocations to instantonlike topological objects. The number of these instantonlike objects depend on the gradient flow kernel. In the case of step-scaling calculations of the lattice β function, the simulations are carried out in the chiral limit where a nonzero instanton number is suppressed. Hence instantonlike objects created by the gradient flow are lattice artifacts. Our investigations reveal a clear correlation between a nonzero topological charge seen by the gradient flow and an increase in the value of gradient flow renormalized coupling. We further demonstrate that this also results in an overestimate of the step-scaling β-function. By investigating the $N_f = 10$ system simulated with domain wall fermions and the $N_f = 8$ system studied with staggered fermions, we show that this artifact is not related to the lattice actions used in the simulations but an artifact of the gradient flow which arises at (very) strong coupling. In both systems we also observe that the effect is more pronounced when using Symanzik compared to Wilson flow.

Since this effect becomes only noticeable at very strong coupling, it may explain why it has not been reported earlier. In the case of our $N_f = 12$ simulations, we checked that both step-scaling calculations using domain wall [10,13,65] or staggered fermions [9] do not include ensembles exhibiting more than one or two configurations where a gradient flow finds nonzero topological charge. These simulations have simply been performed at weaker coupling.

Similarly to step-scaling calculations, continuous β function determinations [66–68] at (very) strong coupling might also be affected by nonzero topological charge occurring as part of the gradient flow. Our studies of the $N_f = 2$ and 12 systems, however, do not extend into the problematic range and are therefore not affected.

ACKNOWLEDGMENTS

We are very grateful to Peter Boyle, Guido Cossu, Anontin Portelli, and Azusa Yamaguchi who develop the GRID software library providing the basis of this work and who assisted us in installing and running GRID on different architectures and computing centers. We thank David Schaich for his support to run additional Symanzik flow measurements on the $N_f = 8$ staggered configurations of Ref. [6]. We benefited from many discussions with Thomas DeGrand, Ethan Neil, and Benjamin Svetitsky. A. H. and O. W. acknowledge support by DOE Grant No. DE-SC0010005. A. H. would like to acknowledge the Mainz Institute for Theoretical Physics (MITP) of the Cluster of Excellence PRISMA+ (Project ID 39083149) for enabling us to complete a portion of this work. O. W. acknowledges partial support by the Munich Institute for Astro- and Particle Physics (MIAPP) which is funded by the Deutsche Forschungsgemeinschaft (DFG, German Research Foundation) under Germany's Excellence Strategy—EXC-2094–390783311. Computations for this work were carried out in part on facilities of the USQCD Collaboration, which are funded by the Office of Science of the U.S. Department of Energy and the RMACC Summit supercomputer [69], which is supported by the National Science Foundation (Grant No. ACI-1532235 and No. ACI-1532236), the University of Colorado Boulder, and Colorado State University. This work used the Extreme Science and Engineering Discovery Environment (XSEDE), which is supported by National Science Foundation Grant No. ACI-1548562 [70] through allocation TG-PHY180005 on the XSEDE resource `stampede2`. This research also used resources of the National Energy Research Scientific Computing Center (NERSC), a U.S. Department of Energy Office of Science User Facility operated under Contract No. DE-AC02-05CH11231. We thank Fermilab, Jefferson Lab, NERSC, the University of Colorado Boulder, Texas Advanced Computing Center (TACC), the NSF, and the U.S. DOE for providing the facilities essential for the completion of this work.

[1] R. Narayanan and H. Neuberger, J. High Energy Phys. 03 (2006) 064.
[2] M. Lüscher, Commun. Math. Phys. **293**, 899 (2010).
[3] M. Lüscher, J. High Energy Phys. 08 (2010) 071.
[4] Z. Fodor, K. Holland, J. Kuti, D. Nogradi, and C. H. Wong, J. High Energy Phys. 11 (2012) 007.
[5] Z. Fodor, K. Holland, J. Kuti, S. Mondal, D. Nogradi, and C. H. Wong, J. High Energy Phys. 09 (2014) 018.
[6] A. Hasenfratz, D. Schaich, and A. Veernala, J. High Energy Phys. 06 (2015) 143.
[7] M. Dalla Brida, P. Fritzsch, T. Korzec, A. Ramos, S. Sint, and R. Sommer (ALPHA Collaboration), Phys. Rev. D **95**, 014507 (2017).
[8] A. Ramos and S. Sint, Eur. Phys. J. C **76**, 15 (2016).
[9] A. Hasenfratz and D. Schaich, J. High Energy Phys. 02 (2018) 132.
[10] A. Hasenfratz, C. Rebbi, and O. Witzel, Phys. Lett. B **798**, 134937 (2019).
[11] Z. Fodor, K. Holland, J. Kuti, D. Nogradi, and C. H. Wong, Phys. Lett. B **779**, 230 (2018).
[12] Z. Fodor, K. Holland, J. Kuti, D. Nogradi, and C. H. Wong, Proc. Sci., LATTICE2019 (**2019**) 121 [arXiv:1912.07653].
[13] A. Hasenfratz, C. Rebbi, and O. Witzel, Phys. Rev. D **100**, 114508 (2019).
[14] A. Hasenfratz, C. Rebbi, and O. Witzel, Phys. Rev. D **101**, 114508 (2020).
[15] M. Lüscher, Commun. Math. Phys. **85**, 39 (1982).
[16] A. Phillips and D. Stone, Commun. Math. Phys. **103**, 599 (1986).
[17] M. Teper, Phys. Lett. B **171**, 86 (1986).
[18] Y. Iwasaki and T. Yoshie, Phys. Lett. **131B**, 159 (1983).
[19] M. Garcia Perez, A. Gonzalez-Arroyo, J. R. Snippe, and P. van Baal, Nucl. Phys. **B413**, 535 (1994).
[20] A. Hasenfratz and C. Nieter, Phys. Lett. B **439**, 366 (1998).
[21] T. A. DeGrand and A. Hasenfratz, Phys. Rev. D **64**, 034512 (2001).
[22] T. A. DeGrand, A. Hasenfratz, and T. G. Kovacs, Phys. Rev. D **67**, 054501 (2003).
[23] C. Alexandrou, A. Athenodorou, and K. Jansen, Phys. Rev. D **92**, 125014 (2015).
[24] C. Alexandrou, A. Athenodorou, K. Cichy, A. Dromard, E. Garcia-Ramos, K. Jansen, U. Wenger, and F. Zimmermann, Eur. Phys. J. C **80**, 424 (2020).
[25] C. Bonati and M. D'Elia, Phys. Rev. D **89**, 105005 (2014).
[26] H. Leutwyler and A. V. Smilga, Phys. Rev. D **46**, 5607 (1992).
[27] P. Hasenfratz, V. Laliena, and F. Niedermayer, Phys. Lett. B **427**, 125 (1998).
[28] T. Schäfer and E. V. Shuryak, Rev. Mod. Phys. **70**, 323 (1998).
[29] C. Bernard, T. A. DeGrand, A. Hasenfratz, C. E. Detar, J. Osborn, S. A. Gottlieb, E. Gregory, D. Toussaint, A. Hart, U. M. Heller, J. Hetrick, and R. L. Sugar, Phys. Rev. D **68**, 114501 (2003).
[30] L. Del Debbio, L. Giusti, and C. Pica, Phys. Rev. Lett. **94**, 032003 (2005).
[31] S. Dürr, Z. Fodor, C. Hoelbling, and T. Kurth, J. High Energy Phys. 04 (2007) 055.
[32] M. Bruno, S. Schaefer, and R. Sommer (ALPHA Collaboration), J. High Energy Phys. 08 (2014) 150.
[33] S. Aoki, G. Cossu, H. Fukaya, S. Hashimoto, and T. Kaneko (JLQCD Collaboration), Prog. Theor. Exp. Phys. (**2018**), 043B07.
[34] P. Fritzsch, A. Ramos, and F. Stollenwerk, Proc. Sci., Lattice2013 (**2014**) 461 [arXiv:1311.7304].
[35] S. Borsanyi, S. Dürr, Z. Fodor, C. Hoelbling, S. D. Katz, S. Krieg, T. Kurth, L. Lellouch, T. Lippert, C. McNeile, and K. K. Szabo, J. High Energy Phys. 09 (2012) 010.
[36] R. Sommer, Proc. Sci., LATTICE2013 (**2014**) 015 [arXiv:1401.3270].
[37] O. Witzel, Proc. Sci., LATTICE2018 (**2019**) 006 [arXiv:1901.08216].
[38] R. C. Brower, A. Hasenfratz, E. T. Neil, S. Catterall, G. Fleming, J. Giedt, E. Rinaldi, D. Schaich, E. Weinberg, and O. Witzel (USQCD Collaboration), Eur. Phys. J. A **55**, 198 (2019).
[39] Z. Fodor, K. Holland, J. Kuti, D. Nogradi, C. Schroeder, and C. H. Wong, Phys. Lett. B **718**, 657 (2012).
[40] Z. Fodor, K. Holland, J. Kuti, S. Mondal, D. Nogradi, and C. H. Wong, J. High Energy Phys. 09 (2015) 039.
[41] Z. Fodor, K. Holland, J. Kuti, S. Mondal, D. Nogradi, and C. H. Wong, Phys. Rev. D **94**, 014503 (2016).
[42] T. Appelquist, R. Brower, G. Fleming, J. Kiskis, M. Lin, E. Neil, J. Osborn, C. Rebbi, E. Rinaldi, D. Schaich, C. Schroeder, S. Syritsyn, G. Voronov, P. Vranas, E. Weinberg, and O. Witzel (Lattice Strong Dynamics Collaboration), Phys. Rev. D **90**, 114502 (2014).
[43] T. Appelquist, R. Brower, G. Fleming, A. Gasbarro, A. Hasenfratz, X.-Y. Jin, E. Neil, J. Osborn, C. Rebbi, E. Rinaldi, D. Schaich, P. Vranas, E. Weinberg, and O. Witzel (Lattice Strong Dynamics Collaboration), Phys. Rev. D **99**, 014509 (2019).
[44] Y. Aoki, T. Aoyama, E. Bennett, M. Kurachi, T. Maskawa, K. Miura, K.-i. Nagai, H. Ohki, E. Rinaldi, A. Shibata, K. Yamawaki, and T. Yamazaki (LatKMI Collaboration), Phys. Rev. D **96**, 014508 (2017).
[45] Y. Aoki, T. Aoyama, M. Kurachi, T. Maskawa, K.-i. Nagai, H. Ohki, A. Shibata, K. Yamawaki, and T. Yamazaki (LatKMI Collaboration), Phys. Rev. D **87**, 094511 (2013).
[46] R. Brower, A. Hasenfratz, C. Rebbi, E. Weinberg, and O. Witzel, Proc. Sci., LATTICE2014 (**2014**) 254 [arXiv:1411.3243].
[47] R. C. Brower, A. Hasenfratz, C. Rebbi, E. Weinberg, and O. Witzel, Phys. Rev. D **93**, 075028 (2016).
[48] A. Hasenfratz, C. Rebbi, and O. Witzel, Phys. Lett. B **773**, 86 (2017).
[49] O. Witzel, A. Hasenfratz, and C. Rebbi, *13th Conference on the Intersections of Particle and Nuclear Physics* (2018) [arXiv:1810.01850].
[50] O. Witzel and A. Hasenfratz (Lattice Strong Dynamics Collaboration), Proc. Sci., LATTICE2019 (**2019**) 115 [arXiv:1912.12255].
[51] W. Detmold, R. G. Edwards, J. J. Dudek, M. Engelhardt, H.-W. Lin, S. Meinel, K. Orginos, and P. Shanahan (USQCD Collaboration), Eur. Phys. J. A **55**, 193 (2019).
[52] C. Morningstar and M. J. Peardon, Phys. Rev. D **69**, 054501 (2004).
[53] Y. Shamir, Nucl. Phys. **B406**, 90 (1993).
[54] V. Furman and Y. Shamir, Nucl. Phys. **B439**, 54 (1995).

[55] R. C. Brower, H. Neff, and K. Orginos, Comput. Phys. Commun. **220**, 1 (2017).
[56] M. Lüscher and P. Weisz, Phys. Lett. **158B**, 250 (1985).
[57] M. Lüscher and P. Weisz, Commun. Math. Phys. **97**, 59 (1985); **98**, 433(E) (1985).
[58] https://github.com/paboyle/Grid.
[59] P. Boyle, A. Yamaguchi, G. Cossu, and A. Portelli, Proc. Sci., LATTICE2015 (**2015**) 023 [arXiv:1512.03487].
[60] S. Duane, A. Kennedy, B. Pendleton, and D. Roweth, Phys. Lett. B **195**, 216 (1987).
[61] U. Wolff (ALPHA Collaboration), Comput. Phys. Commun. **156**, 143 (2004).
[62] A. Hasenfratz and F. Knechtli, Phys. Rev. D **64**, 034504 (2001).
[63] A. Hasenfratz, R. Hoffmann, and S. Schaefer, J. High Energy Phys. 05 (2007) 029.
[64] T. Appelquist, R. Brower, G. Fleming, A. Hasenfratz, X.-Y. Jin, J. Kiskis, E. Neil, J. Osborn, C. Rebbi, E. Rinaldi, D. Schaich, P. Vranas, E. Weinberg, and O. Witzel (Lattice Strong Dynamics Collaboration), Phys. Rev. D **93**, 114514 (2016).
[65] A. Hasenfratz, C. Rebbi, and O. Witzel, Proc. Sci., LATTICE2018 (**2019**) 306 [arXiv:1810.05176].
[66] A. Hasenfratz and O. Witzel, Phys. Rev. D **101**, 034514 (2020).
[67] A. Hasenfratz and O. Witzel, Proc. Sci., LATTICE2019 (**2019**) 094 [arXiv:1911.11531].
[68] Z. Fodor, K. Holland, J. Kuti, D. Nogradi, and C. H. Wong, EPJ Web Conf. **175**, 08027 (2018).
[69] J. Anderson, P. J. Burns, D. Milroy, P. Ruprecht, T. Hauser, and H. J. Siegel, *PEARC17: Proceedings of the Practice and Experience in Advanced Research Computing 2017 on Sustainability, Success and Impact July 2017* Article No.: 8 (2017), pp. 1–7, https://doi.org/10.1145/3093338.3093379.
[70] J. Towns, T. Cockerill, M. Dahan, I. Foster, K. Gaither, A. Grimshaw, V. Hazlewood, S. Lathrop, D. Lifka, G. D. Peterson, R. Roskies, J. R. Scott, and N. Wilkins-Diehr, Comput. Sci. Eng. **16**, 62 (2014).